Applied Thermal Engineering 106 (2016) 1225–1235

Contents lists available at ScienceDirect

Applied Thermal Engineering

journal homepage: www.elsevier.com/locate/apthermeng

Experimental and numerical investigation of natural convection in a double skin facade

Tuğba İnan [a,*], Tahsin Başaran [a], Mehmet Akif Ezan [b]

[a] Department of Architecture, Izmir Institute of Technology, 35430 İzmir, Turkey
[b] Department of Mechanical Engineering, Dokuz Eylul University, 35397 Izmir, Turkey

HIGHLIGHTS

- Flow and thermal profile were obtained inside a cavity ($8.59E09 \leqslant Ra \leqslant 1.41E10$).
- Heat flux and *Nu* distributions along the cavity height were obtained.
- A correlation was generalized by using *Nu* and *Ra* numbers.

ARTICLE INFO

Article history:
Received 16 February 2016
Revised 15 June 2016
Accepted 18 June 2016
Available online 20 June 2016

Keywords:
Natural convection
Double skin facade
Differentially heated cavity
Closed cavity

ABSTRACT

In this study, airflow and heat transfer in a rectangular cavity that simulates a double skin facade and includes natural convection were examined numerically and experimentally. This cavity separates the exterior space and the thermally controlled interior space. The temperatures of the surfaces that interact with these spaces were determined experimentally, while the other surfaces were regarded as adiabatic. With these temperature values, the parameters of the numerical study were defined. After the validation of the numerical model was completed based on experimental studies in the literature, the results related to flow and heat transfer in the cavity were analyzed. The numerical model provided results that agree with the air temperature values found experimentally in the cavity. Accordingly, in natural convection, with Rayleigh numbers ranging from $8.59 * 10^9$ to $1.41 * 10^{10}$ and the effect of buoyancy on the regions close to the surface, the increasing tendency of the average Nusselt number from 142.6 to 168.8 was shown. In addition, a correlation between the Rayleigh and Nusselt numbers for a cavity aspect ratio of 8.64 was constructed to evaluate the heat flux; this correlation was also shown graphically.

1. Introduction

Sustainability and the corresponding search for sustainable buildings increasingly occupy a significant role in architecture. At both the national and international scale, this concern has led authorities to redefine building performance standards and requires a revision of architectural thinking. In this respect, in architectural discourse, it is possible to notice an increasing interest in building skin configurations that promise to help minimize the loss of energy while maximizing energy gain. In parallel, it is possible to see that the use of double skin glass facades has become globally prevalent. The basic assumption behind this global proliferation is that considering climatic conditions, double skin glass facades can provide the advantages of energy gain and controlled ventilation. A double skin facade system consists of an external glass skin and an internal glass skin. An air duct called a cavity is located between these two skins. The size of the air cavity can vary from 20 cm to 2 m, and a shading system can be positioned inside the cavity. This facade system can be grouped into different categories according to the ventilation type [1]. The cavity is ventilated by airflow that is driven either by buoyancy forces or by mechanical devices. In a double skin facade system, air movement between the two glass skins can be performed according to various air flow modes. In one of these groups, which is named a "buffer zone," both the interior and exterior facade surfaces are airproof. That is, there is no air movement from the exterior environment to the cavity or from the cavity to the outside, and there is a temperature difference between the interior and exterior surfaces. This phenomenon of differentially heated/cooled cavities has been studied extensively in the literature [2–13]. On the other hand, some double skin facade applications have been designed considering open cavity natural convection [14–18].

* Corresponding author.
E-mail addresses: tugbainan85@gmail.com, tugbainan@iyte.edu.tr (T. İnan).

http://dx.doi.org/10.1016/j.applthermaleng.2016.06.124
1359-4311/

Nomenclature

CA	cavity air
c_p	specific heat, J/kg K
DSF	double skin facade
g	gravitational acceleration, m/s^2
H	geometric height, m
k	thermal conductivity, W/mK; local turbulence kinetic energy
L	geometric length, m
Nu	Nusselt number
p	pressure, Pa
PFOG	primary facade outer glass
r	radial coordinate; internal radius, m
Ra	Rayleigh number
q''	heat flux, W/m^2
SFIG	secondary facade inner glass
t	time, s
T	temperature, °C
u	velocity, x-direction, m/s
v	velocity, y-direction, m/s
w	velocity, z-direction, m/s
W	geometric length, m
x, y, z	coordinate axis

Greek symbols

α	thermal diffusivity m^2/s
β	volumetric thermal expansion coefficient, 1/K
ε	diffusion rate
μ	dynamic viscosity, kg/m s
ν	kinematic viscosity, m^2/s
ρ	density, kg/m^3
Δ	differential element

Superscripts

C	cold
H	hot
t	turbulence

Many numerical and experimental studies related to airproof double skin facades (DSFs) with an enclosed cavity have also been carried out in the literature [7,19,20]. Betts and Bokhari [7] experimentally investigated the natural convection of air in a tall rectangular cavity that is differentially heated. The mean and turbulent temperature and velocity variations within the cavity were measured along with the heat fluxes. The results provide a benchmark for the testing of turbulence models in the low turbulence Reynolds number range of $0.86 * 10^6$–$1.43 * 10^6$. Xaman et al. [19] numerically studied fluid flow and heat transfer in a DSF with natural convection using laminar ($10^2 \leqslant Ra \leqslant 10^6$) and turbulent ($10^4 \leqslant Ra \leqslant 10^8$) models. They constructed different correlations including Nu and Ra numbers for different aspect ratios (height/width). Missoum et al. [20] numerically studied heat exchange by convection and conduction between two environments of a building separated by a vertical wall and double wall air cavity for different Rayleigh numbers ($10^3 \leqslant Ra \leqslant 10^7$). On the other hand, Manz investigated natural convection for an open cavity double skin facade [14]. He studied a naturally ventilated DSF with an external air curtain, and the DSF cavity had a mid-pane shading device for summer conditions. He found the effect of the solar device position within the DSF cavity and the effects of the cavity ventilation characteristics on the total solar energy transmittance (g). In the study, a CFD tool was used for the simulations, and the CFD simulation results were compared with measurements. The results showed that having a solar protective layer on the exterior facade is more effective than having this layer on the interior facade. However, it was found that partially closing both solar shades provided more air ventilation in the DSF and a lower g value. Fossa et al. [15] carried out an experimental study on natural convection in an open channel to investigate the effect of the geometric configuration of electrical heat sources on one side of the cavity. They found the local and average Nusselt numbers using experimental data and generated a correlation with the Rayleigh numbers. Pappas and Zhai [16] made an integrated and iterative model to analyze the thermal performance of a DSF cavity with buoyancy-driven airflow using a building energy simulation program and a computational fluid dynamics (CFD) package. After validation, they compared the results of these numerical programs and found the results to be reasonably close to each other; they then developed a linear correlation using two programs. Kuznik et al. [17] experimentally studied different airflow rates through the facade air channels and different angles of the solar shading devices in summer. A sensitivity analysis was carried out using different CFD modeling strategies for a naturally ventilated cavity to predict flow and temperature patterns through the cavity in Pasut and De Carli's study [18]. Different turbulence models and 2D/3D geometries were compared to highlight the advantages and disadvantages of each approach. After validating the numerical model using experimental data, they showed that the 2D model has reasonable accuracy compared to the 3D model. The results of k-ε RNG model were found to be satisfactory compared to the k-ω SST model.

The above studies related to an enclosed cavity for an airproof double skin facade mainly have low Rayleigh numbers. However, Rayleigh numbers are larger than 10^{10} in some studies [10–13]. Trias et al. [10,11] studied different Rayleigh numbers from $6.4 * 10^8$ to 10^{11}. Saury et al. [12] analyzed natural convection in an air cavity with experimental results at large Rayleigh numbers of up to $1.2 * 10^{11}$. Velocity and temperature measurements were taken throughout the whole cavity. They examined airflow inside the cavity and the Nusselt number along the hot and the cold wall surfaces. The Rayleigh number was $4.6 * 10^{10}$ for the study by Lau et al. [13]. The aspect ratios of the cavities were different for these studies.

The studies show that a combination of experiments and simulations provides more reliable results for analyzing DSFs. In the present study, flow and heat transfer in a rectangular cavity that simulates a double skin facade and includes natural convection were examined numerically experimentally. A full-scale experimental setup was built, and the aspect ratio of the cavity was 8.64. The numerical model was validated based on existing experimental studies in the literature, and the results were examined in relation to the flow and heat transfer in the cavity. With natural convection, considering the Rayleigh number obtained for this study and the effect of buoyancy on the regions near the heat transfer surfaces, the tendency of the Nusselt numbers to increase was demonstrated. Furthermore, along with the increasing Rayleigh numbers, corresponding increases in the Nusselt numbers were shown. In addition, a correlation based on both Rayleigh and Nusselt numbers was determined for an airproof double skin facade cavity in the range of $8.59 * 10^9 \leqslant Ra \leqslant 1.41 * 10^{10}$.

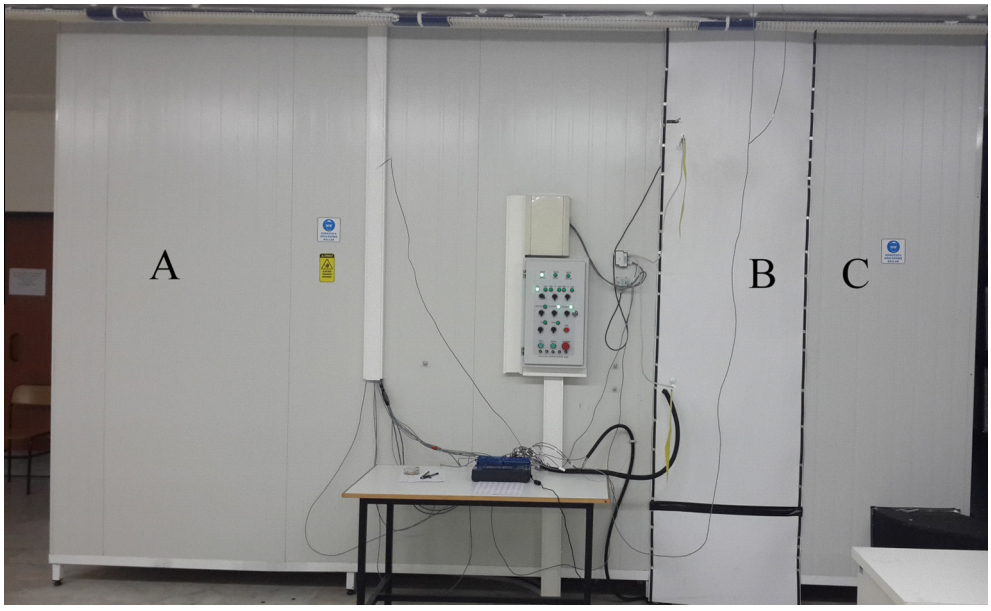

Fig. 1. General view of the experimental setup.

2. Experimental setup

The experimental setup was placed at the Building Physics Laboratory, which is 11.9 m in width, 17.8 m in length and 4 m in height, on the ground floor of Block B of the Faculty of Architecture, İzmir Institute of Technology. A general view of the experimental setup in the laboratory is shown in Fig. 1. The experimental study included flow and heat transfer analysis for the buffer zone condition of the double skin facade (B) between the indoor (A) and outdoor (C) environmental conditions. While the indoor environment was conditioned with a heating or cooling bath using water, the outdoor environment was conditioned directly with a cooling group placed outside the building.

Fig. 2 shows a general view of the experimental setup. The Indoor Environment Simulation Setup shown as A in Figs. 1 and 2, which is 1.5 m in width, 3 m in length and 3 m in height, was manufactured using 10-cm-thick polyurethane thermal insulation panels. One of the short walls was double-glazed with dimensions of 4–12–4 mm. A thermally insulated door was placed on the other short side wall of the indoor environment setup. Heating/cooling serpentines 2.5 m long and made of thin aluminum sheets around copper pipes were used to circulate water from the cooling-heating bath can and were placed on the long walls of the setup to face each other (Fig. 2). The water temperature was maintained at the desired temperature by a thermostat located in the room.

The Outdoor Environment Simulation Setup shown as C in Figs. 1 and 2, which was 1.5 m in width, 0.9 m in length and 3 m in height, was manufactured using 10-cm-thick polyurethane thermal insulation panels, similar to the indoor environment. One surface was single-glazed with a 4-mm–thick pane. The other surface was in contact with the double skin facade cavity that separates the indoor and outdoor environments of the experiment room from each other. The cooling of the environment was performed with cooling serpentines hung on the two opposite wall surfaces (Fig. 2). The outer unit of the cooling system was located outside the building and maintained the environment at the required temperature by directly circulating the refrigerant through the serpentines.

The experimental room intermediate partition was designed to simulate the double facade, as shown by B in Figs. 1 and 2. A single-glazed glass component 4 mm thick on the outer surface of the double facade was mounted on the mechanism of this system positioned between the outdoor and indoor environments

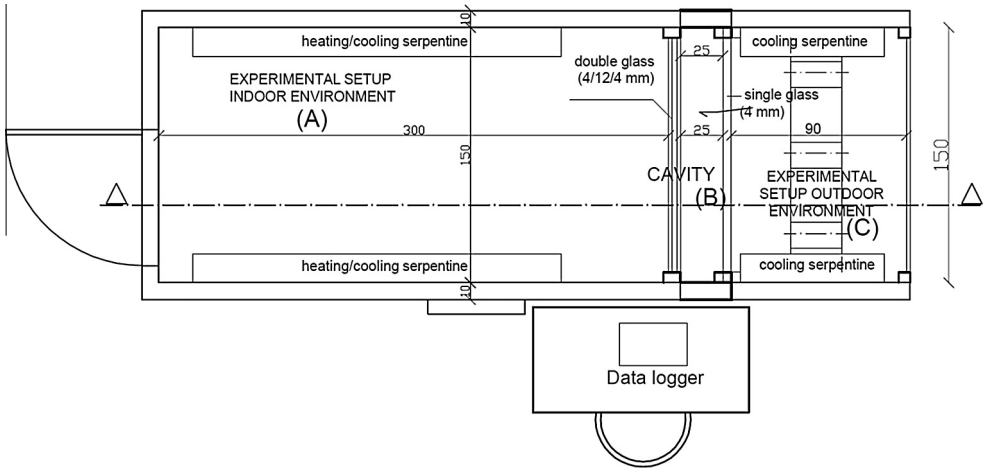

Fig. 2. Plan view of the experimental setup.

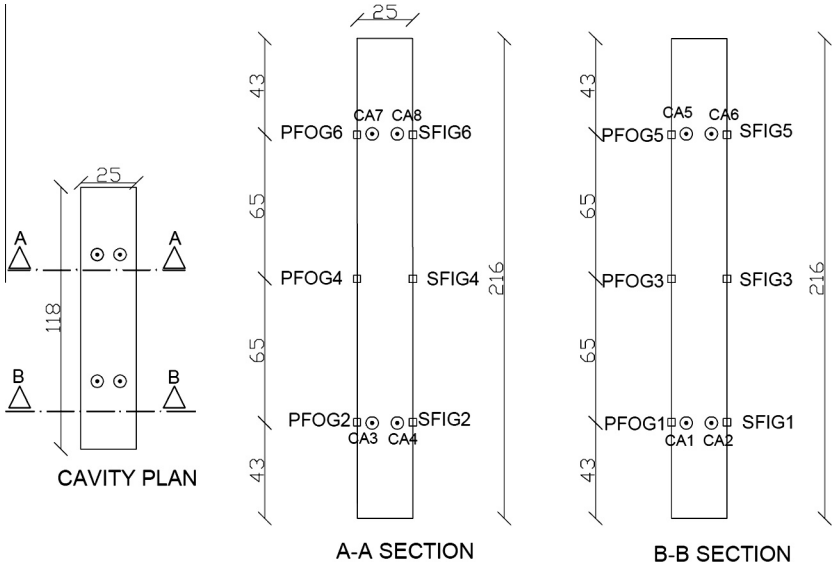

Fig. 3. Layout of the thermocouples in the cavity.

of the experiment room. The other surface of the intermediate region was empty and overlapped with the double skin facade of the indoor environment. The cavity was highly insulated against heat transfer. Thus, the outdoor and indoor environment simulation setup dimensions decreased from 3 m in height and 1.5 m in width to 2.16 m in height and 1.5 m in width. The cavity was closed, and only natural convection was considered. The difference in the dimensions is related to the additional insulation. The insulation provided one-dimensional heat transfer through only the glass.

Temperature measurements at different points of the experimental setup were taken with the T-type thermocouples mentioned Fig. 3 and were recorded with the data logger (HIOKI LR 8402-20) shown in Figs. 1 and 2. Eight thermocouples were placed inside the cavity to determine the variation of the air temperature in the cavity. The layout of the thermocouples in the cavity is shown in Fig. 3; the thermocouples are numbered from CA1 (cavity air) to CA8. Six T-type thermocouples each were placed on two different surfaces to measure the inner surface temperatures of the double skin facade. These thermocouples are numbered in Fig. 3 from PFOG1 (primary facade outer glass) to PFOG6 for the portion of the cavity facing the inner room and from SFIG1 (secondary facade inner glass) to SFIG6 for the portion of the cavity facing the outer room. Except for these temperature measurements, the temperatures that simulate the indoor and outdoor environments were measured at different points. These temperature measurements were used to determinate the steady state condition of the experiments.

The calibration of each of the thermocouples used in the experimental setup were performed in the calibration laboratories of İzmir Chamber of Mechanical Engineers (KALMEM). The calibration of the thermocouples was performed using a PT 100 probe connected to an HP 3458 multimeter, both of which were calibrated in the National Metrology Institute of Turkey. The total uncertainty of the calibrated thermocouples and the data logger was estimated to be ±0.034 °C.

3. Experimental results

In this study, seven experimental measurements were taken. At the start of each test, the experimental setup was run for a different time period at steady state conditions before the measurements were taken. The temperature values at each point in the cavity, as shown in Fig. 3, were recorded at 2-s intervals. For the first experimental result, the changes in the average temperatures on the interior surfaces of the cavity are shown in Fig. 4. Accordingly, the system that was thermally stable in the beginning, based on the different temperatures on the interior and exterior, became stable after some time. Because the part that simulates the exterior environment was relatively colder, a temperature difference existed between the two interior surfaces of the cavity. The temperature values on the interior of the surface facing the exterior space of the cavity reflect the average value of the six thermocouples (SFIG1-6) after the temperature stabilized. Thermocouples PFOG1–6 give the average temperature values of the interior of the surface facing the interior cavity space.

The surface temperature averages given in Fig. 4 come from six thermocouples and are used in the calculation of the Rayleigh numbers (*Ra*). Along the interior glass surfaces of the cavity, temperature changes occur. This change is shown in Fig. 5. Each point refers to the average of two thermocouples placed at the same height of the cavity. As shown in Fig. 5, the temperature values increase depending on the height. The figure also shows the linear equality that clearly reflects this change. In the numerical study, as a boundary condition, these changes in the temperature were considered, and these linear equations were used.

For the first experimental results, to show the oscillation of the temperature values due to the activation of the cooling and heating

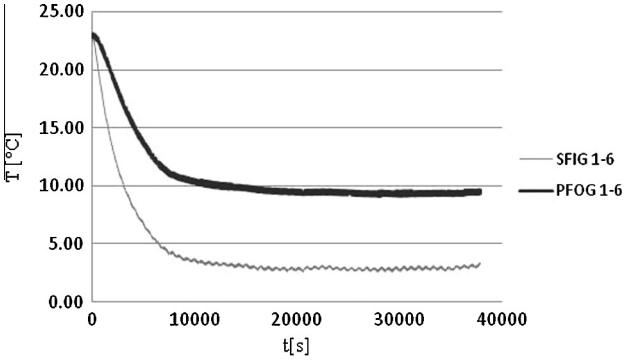

Fig. 4. Variation of temperature in the cavity surfaces for the first experiment.

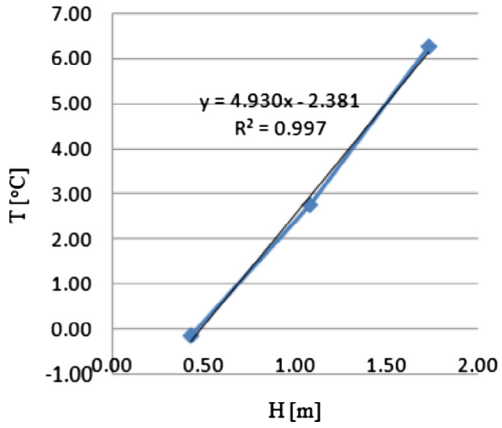

(a) Secondary facade inner glass (SFOG)

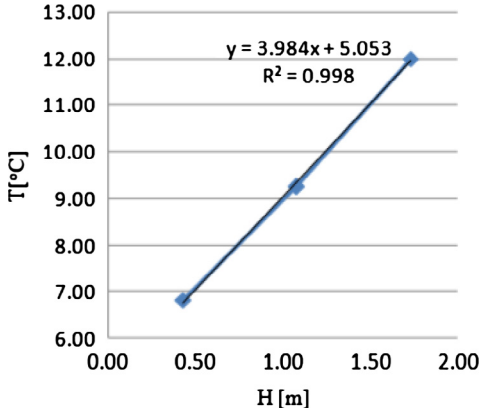

(b) Primary facade outer glass (PFOG)

Fig. 5. Variation of temperature in both interior surfaces along the cavity height for the first experiment.

system after the steady state condition, the average temperature changes on the interior surfaces of the cavity are shown in Fig. 6. As shown in Fig. 6, the temperatures were calculated in a very stable way, and the standard deviation for both of the temperature averages is only 0.1 °C.

For the first experimental study, another time-dependent temperature change after the steady state condition is shown in Fig. 7. With the effect of natural convection, the high temperature air is located at the top. "CA1-4" shows the average temperature of the four thermocouples at the bottom, whereas "CA5-8" is the average temperature of the top four thermocouples.

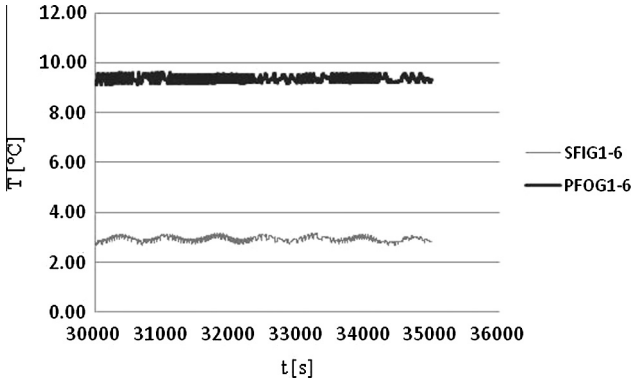

Fig. 6. Variation of temperatures in both inner surfaces along the cavity height for the first experiment.

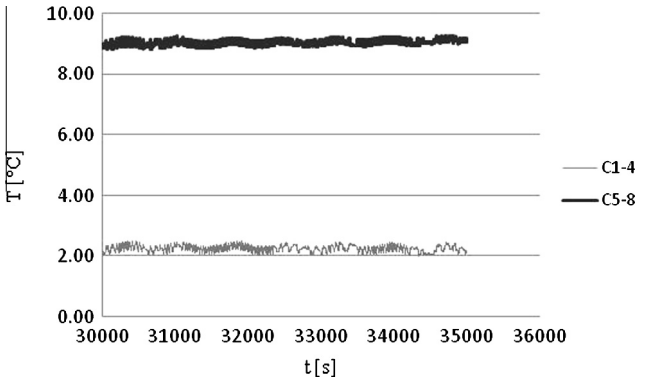

Fig. 7. Variation of air temperature in the cavity for the first experiment.

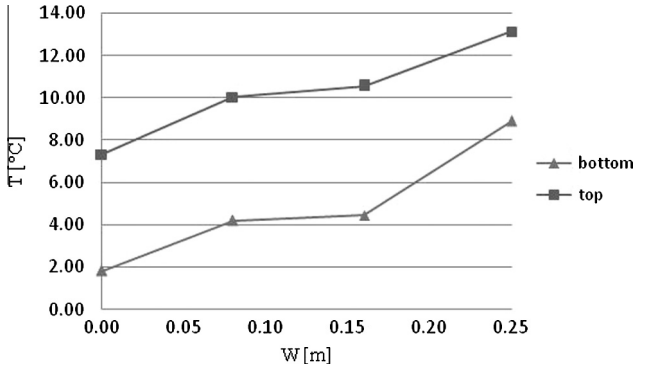

Fig. 8. Variation of temperature in the cavity for the first experiment.

In the first experimental study, the average temperature ranges of the two different height sections of the cavity after the steady state condition are shown in Fig. 8. The two points in the middle give the air temperature, and the temperatures on the sides refer to the average surface temperatures measured by two thermocouples each. Heat transfer occurs due to these temperature differences between the air and the surface. Additionally, the change in the air temperature depending on the height can be observed.

4. Numerical study

4.1. Meshing and solution method

A finite volume–based solver (ANSYS-FLUENT v14.5 [21]) was used to predict the velocity and temperature distributions inside the three-dimensional cavity. A preliminary mesh independency survey revealed that a total of $1.3 * 10^6$ control volumes is optimum considering both the computational time and accuracy. To capture the high gradients near the solid surfaces, the mesh intensity increased close to the walls. Fig. 9 shows the mesh structure of the cavity on the x-y and y-z planes.

The following assumptions were considered in the current study:

- The fluid is Newtonian and incompressible.
- The flow is steady, fully turbulent and three dimensional.
- The thermo-physical properties of the air were assumed to be constant except for the density. The Boussinesq approximation was used to account for the buoyancy term in the momentum equation.
- Viscous dissipation and radiation effects were neglected.

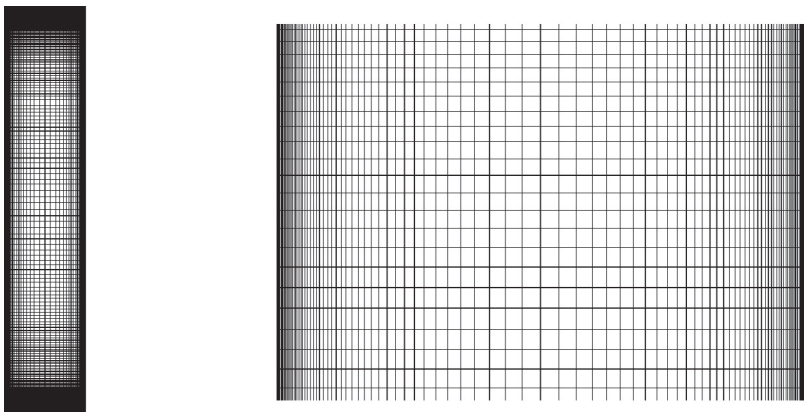

(a) x-y plane general view (b) y-z plane close view

Fig. 9. Grid configurations.

These simplifications reduce the governing equations into following forms:

Mass

$$\frac{\partial}{\partial x}(\rho u)+\frac{\partial}{\partial y}(\rho v)+\frac{\partial}{\partial z}(\rho w)=0 \tag{1}$$

x-momentum

$$\frac{\partial}{\partial x}(\rho uu)+\frac{\partial}{\partial y}(\rho vu)+\frac{\partial}{\partial z}(\rho wu) = -\frac{\partial p}{\partial x}+(\mu+\mu_t)\left[\frac{\partial^2 u}{\partial x^2}+\frac{\partial^2 u}{\partial z^2}+\frac{\partial^2 u}{\partial y^2}\right] \tag{2}$$

y-momentum

$$\frac{\partial}{\partial x}(\rho uv)+\frac{\partial}{\partial y}(\rho vv)+\frac{\partial}{\partial z}(\rho wv) = -\frac{\partial p}{\partial y}+(\mu+\mu_t)\left[\frac{\partial^2 v}{\partial x^2}+\frac{\partial^2 v}{\partial y^2}+\frac{\partial^2 v}{\partial z^2}\right]-\rho g\beta(T_\infty-T) \tag{3}$$

z-momentum

$$\frac{\partial}{\partial x}(\rho uw)+\frac{\partial}{\partial y}(\rho vw)+\frac{\partial}{\partial z}(\rho ww) = -\frac{\partial p}{\partial z}+(\mu+\mu_t)\left[\frac{\partial^2 w}{\partial x^2}+\frac{\partial^2 w}{\partial y^2}+\frac{\partial^2 w}{\partial z^2}\right] \tag{4}$$

Energy

$$\frac{\partial}{\partial x}(\rho uc_pT)+\frac{\partial}{\partial y}(\rho vc_pT)+\frac{\partial}{\partial z}(\rho wc_pT) = \frac{\partial}{\partial x}\left(k\frac{\partial T}{\partial x}\right)+\frac{\partial}{\partial y}\left(k\frac{\partial T}{\partial y}\right)+\frac{\partial}{\partial z}\left(k\frac{\partial T}{\partial z}\right)-\frac{\partial}{\partial x_i}\left(\frac{\partial T}{\partial x_i}\frac{c_p\mu_t}{\sigma_t}\right) \tag{5}$$

Here velocity, pressure and temperature are defined as time-averaged. Turbulence can be determined for each computational node in the domain in terms of the local turbulence kinetic energy (k) and the diffusion rate (ε),

$$\mu_t=\rho C_\mu\frac{k^2}{\varepsilon} \tag{6}$$

To resolve the turbulence energy and diffusion rate terms, the Realizable k-epsilon turbulence model was used. In comparison to the classical k-epsilon method, the realizable model is more successful and accurate for the problems with flow separation, re-attachment and complicated secondary flows [21]. In the realizable k-epsilon method, the following additional equations are resolved to evaluate the kinetic energy and the dissipation rate,

$$\frac{\partial}{\partial x_j}(\rho ku_j)=\frac{\partial}{\partial x_j}\left[\left(\mu+\frac{\mu_t}{\sigma_k}\right)\frac{\partial k}{\partial x_j}\right]+G_k+G_b-\rho\varepsilon-Y_M+S_K \tag{7}$$

$$\frac{\partial}{\partial x_j}(\rho\varepsilon u_j)=\frac{\partial}{\partial x_j}\left[\left(\mu+\frac{\mu_t}{\sigma_\varepsilon}\right)\frac{\partial\varepsilon}{\partial x_j}\right]+\rho C_1S\varepsilon-\rho C_2\frac{\varepsilon^2}{k+\sqrt{v\varepsilon}}+C_{1\varepsilon}\frac{\varepsilon}{k}C_{3\varepsilon}G_b+S_\varepsilon \tag{8}$$

The details of the terms and constants that are given in the governing equations can be found in the theory book from ANSYS-FLUENT [21]. The SIMPLE algorithm of Patankar [22] was used to solve the pressure-velocity coupling. In the decomposition of the pressure term, the PRESTO method was used, whereas for the other transport equations, the QUICK [23] scheme was applied. In the analyses, for the all of the transport parameters, the convergence criterion has been defined as 10^{-7}.

4.2. The validation of the solution method

To validate the current solution methodology, a similar experimental study from the literature was resolved, and the comparative results are presented. King [4] carried out experimental measurements for natural convection flow inside a tall cavity with dimensions of H = 2.5 m, W = 0.5 m and L = 1.0 m. In the experimental study, the hot and cold surfaces were kept at the temperatures of T_H = 77.2 °C and T_C = 31.4 °C, respectively. According to the geometric and boundary conditions, the corresponding *Ra* number is calculated as 4.6×10^{10}. In the experimental setup, the temperature values inside the cavity were measured by a thermocouple traversing mechanism. A Laser Doppler Anemometer (LDA) system was used to capture the velocity variations near the cavity walls. The temperature measurement sensors have an accuracy of ±0.2 K, and the uncertainty of the velocity measurements is 0.02 m/s. This comprehensive experimental study by King [4] is preferred by various researchers for validating natural convection simulations inside tall cavities [9,13].

The velocity profile and variation of the Nusselt number on the hot surface is compared with the reference study in Fig. 10. Here, both experimental and numerical data were obtained on a mid-surface of z = L/2 and y = H/2. The comparison shows that the numerical results have a similar tendency as the experimental measurements. To validate the predicted velocity field and temperature distributions inside the cavity, another set of comparisons

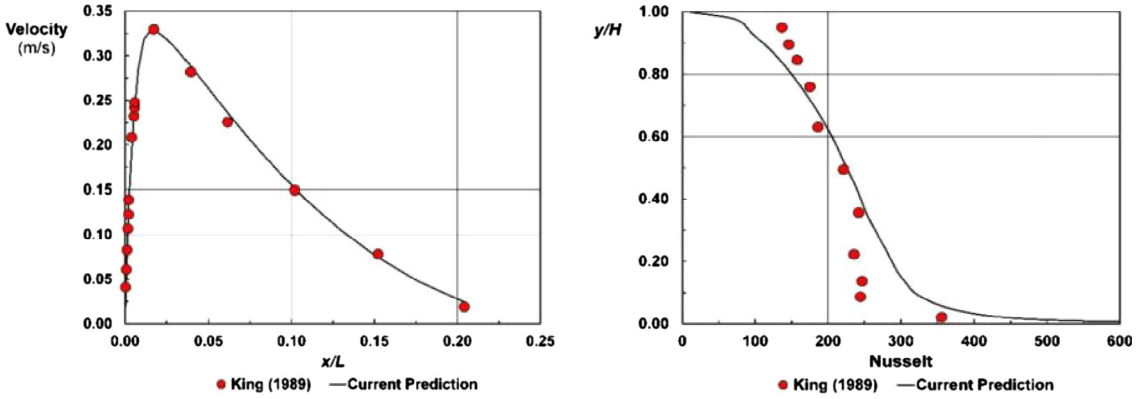

(a) Velocity profile (b) Nusselt variation

Fig. 10. The velocity profile and variation of the Nusselt number on the hot surface.

was conducted based on the numerical results from Lau et al. [13]. Lau et al. [13] conducted an analysis based on time-dependent Large-Eddy-Simulation (LES) as the turbulence model. Although steady state RANS (Reynolds-Averaged Navier Stokes) equations were solved in the current model, similar variations can be seen in Fig. 11.

4.3. Numerical model

In Fig. 12, the reduced geometry of the test room is shown with the boundary conditions. The height, width and depth of the test room were H = 2.16 m, W = 0.25 m and L = 1.18 m. The aspect ratio (H/W) of the cavity was 8.64. Apart from the side surfaces that had constant temperatures of T_H and T_C, all of the surfaces are regarded as adiabatic.

In the experimental studies, along the three lines indicated on the side surfaces of the cavity (y = 0.43 m, 1.08 m and 1.73 m), the temperature values were measured with thermocouples, and the temperature changes were determined for each experiment. The experimental measurement results and the corresponding Rayleigh numbers are presented in Table 1. According to the boundary conditions given in Table 1, the Rayleigh number ranges from $8.59 * 10^9$ to $1.41 * 10^{10}$. Here, the Rayleigh number is defined as

$$Ra_H = \frac{g\beta}{\nu\alpha}(T_H - T_C)H^3 \tag{9}$$

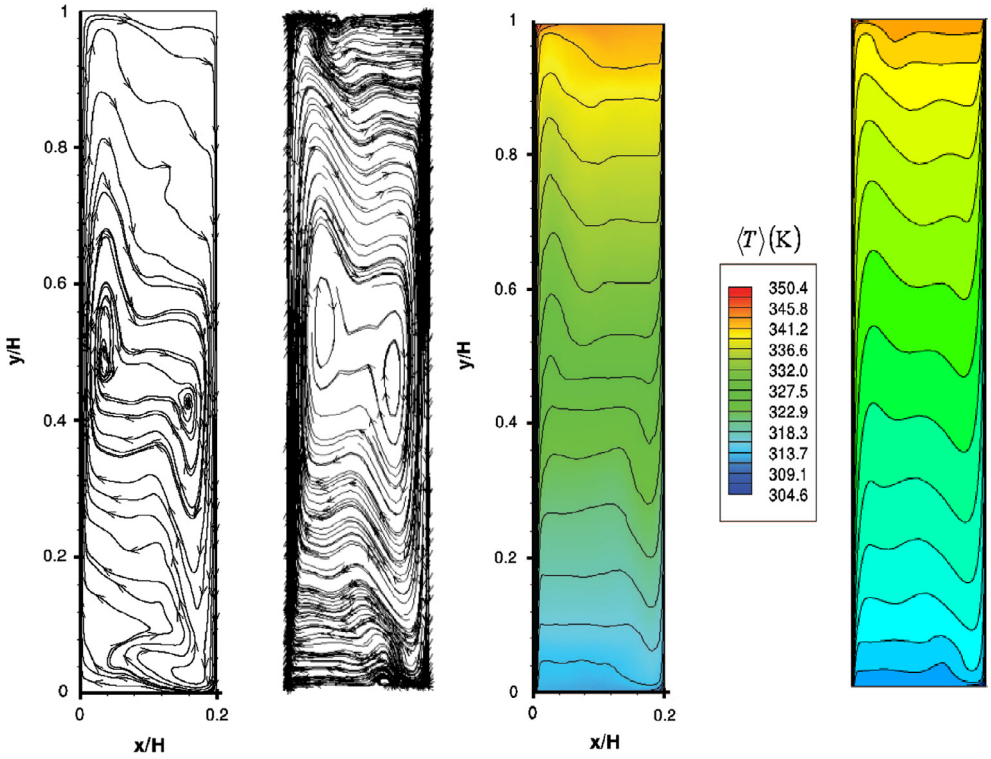

Lau et al. [13] Current model Lau et al. [13] Current model

(a) Streamlines (b) Isotherms

Fig. 11. Velocity and temperature fields on the z = L/2 plane.

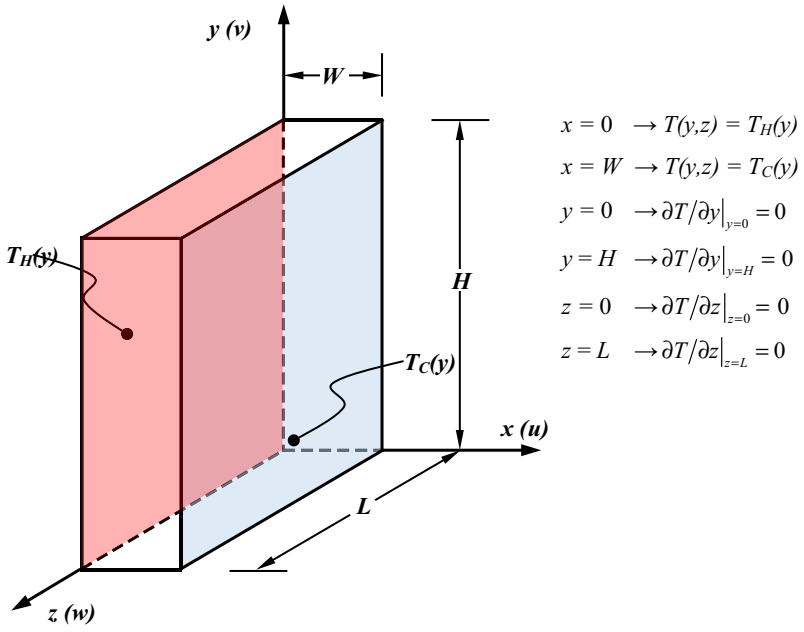

Fig. 12. Test room geometry and boundary conditions.

Table 1
Experimental measurement values and calculated Rayleigh numbers.

Experiment#	*PFOG*			*SFIG*					
	$T_{1,2avg}$	$T_{3,4avg}$	$T_{5,6avg}$	$T_{1,2avg}$	$T_{3,4avg}$	$T_{5,6avg}$	T_C	T_H	*Ra*
1	−0.16	2.74	6.25	6.82	9.25	12.00	2.94	9.36	8.59E+09
2	0.79	3.71	7.35	8.51	11.30	14.22	3.95	11.34	9.74E+09
3	0.89	4.38	8.95	8.96	12.06	16.20	4.74	12.41	1.00E+10
4	1.46	4.80	8.29	10.63	13.67	17.62	4.85	13.97	1.16E+10
5	1.60	5.22	8.90	11.42	14.78	19.32	5.24	15.17	1.25E+10
6	1.97	5.76	9.58	12.48	16.08	21.15	5.77	16.57	1.34E+10
7	2.94	7.03	11.13	14.12	17.91	23.48	7.03	18.50	1.41E+10

where the average temperature values T_H and T_C were determined using the measured surface temperatures SFIG1 to 6 (for T_H) and PFOG1 to 6 (for T_C). The Rayleigh numbers calculated using Eq. (9) increase with increasing temperature values, as shown in Table 1.

5. Results and discussions

According to the boundary conditions given in Table 1, the Rayleigh number ranges from $8.59 * 10^9$ to $1.41 * 10^{10}$. In Fig. 13, the velocity variations along the cavity width are shown at y = 1.73 m for the different experimental conditions. Although the temperature difference inside the cavity changes in each experiment, the velocity variation maintained almost constant at the center of the cavity from 0.05 m to 10.20 m. On the other hand, the air close to the cold and hot surfaces was affected by the buoyancy forces that are caused by the density differences induced by the temperature gradients. Fig. 13 shows that similar velocity variations were obtained at the cold and hot surfaces along the streamwise direction for different *Ra* numbers and that the highest *Ra* number (for the last numerical experiment) was more than double that of the first numerical experiment.

The isotherms on the z = L/2 plane are shown in Fig. 14. Because the Rayleigh number varies in a relatively narrow range, there is not a significant difference in the temperature ranges. However, as the surface temperatures increase along the flow direction, the air temperature also increases, and the hot zones in the cavity expand.

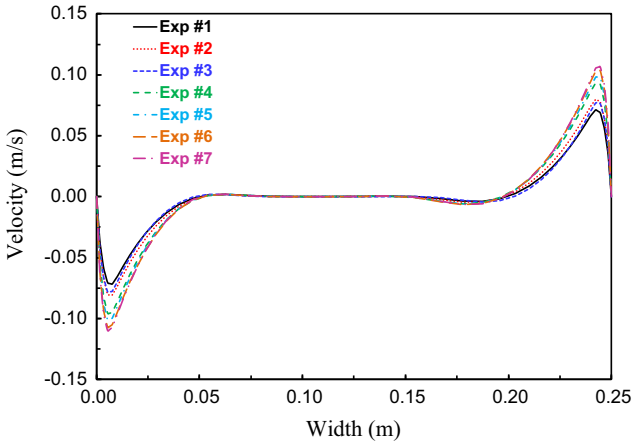

Fig. 13. Velocity variations inside the cavity for different numerical experiments at y = 1.73 m.

In Fig. 15, the temperature variations inside the cavity are compared with the experimental measurements at the height of y = 1.73 m. Different surface temperatures were tested in the experiments, and different temperature-location slopes were created in the cavity. When the dimensionless temperature values

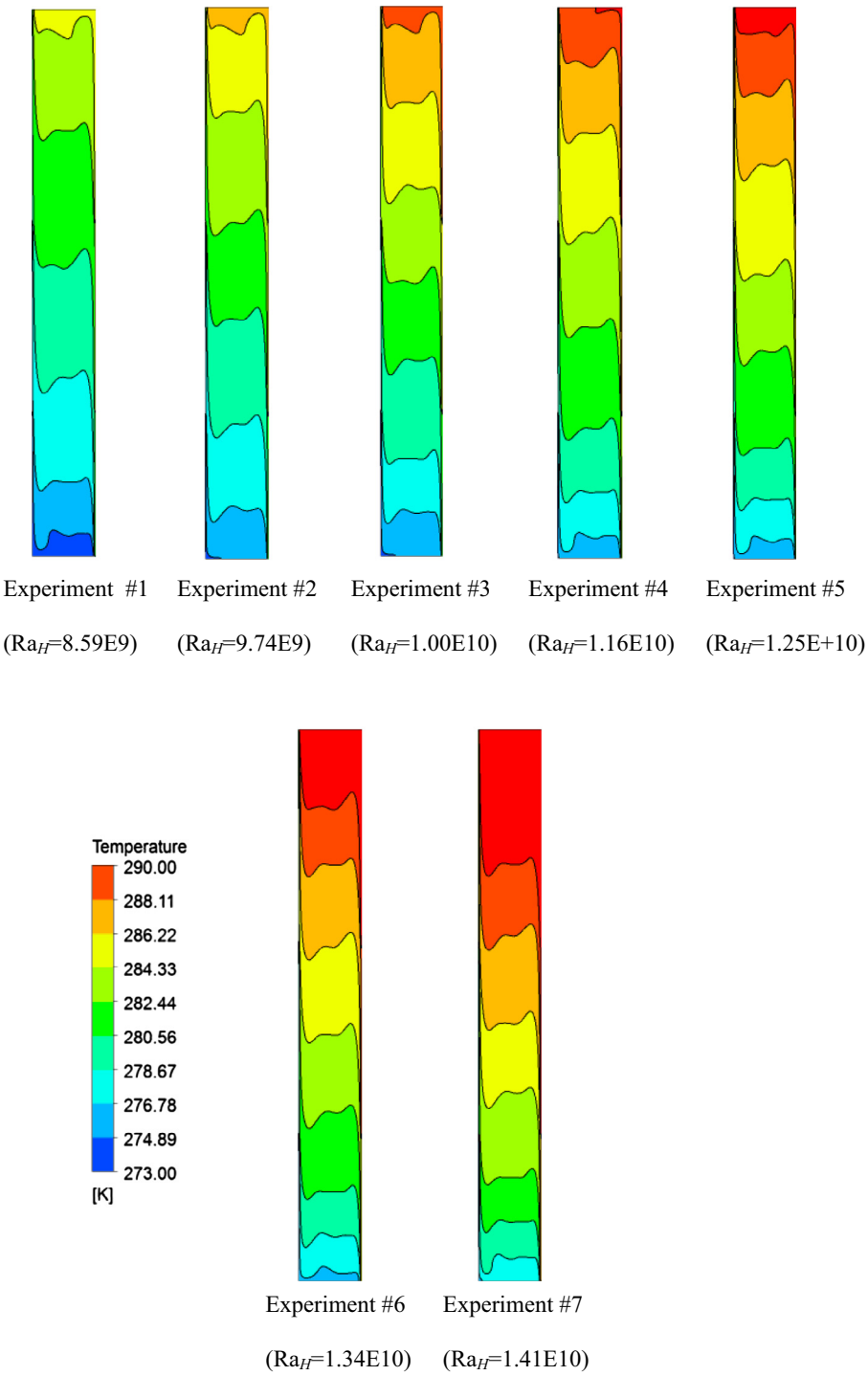

Fig. 14. Temperature variations on the $z = L/2$ plane for different *Ra* numbers.

are taken into account, it is seen that, similar to the velocity ranges, the temperature ranges are identical in form. It is clear that the temperature variations have similar tendencies for each experiment but that they are shifted by varying the Rayleigh number. The temperature measurements from the experiments are also shown in Fig. 15 by solid markers. The experimental results match the numerical results well. The largest difference was less than 1 °C for the comparisons between the numerical and experimental results. These differences could be mainly caused by the measurement point uncertainties for the y-direction as well as for the x- and z–directions, as shown in Fig. 12.

Variations of the heat fluxes along the cavity height at two separate surfaces can be seen in Fig. 16 for different *Ra* numbers. The heat flux values increase with increasing Rayleigh number and reach the maximum and minimum values at the top and bottom of the cavity, respectively.

The Nusselt numbers were also evaluated using the mean heat flux values on the hot surface of the cavity through Eq. (10),

$$Nu_H = \frac{q''}{\Delta T}\frac{H}{k} \tag{10}$$

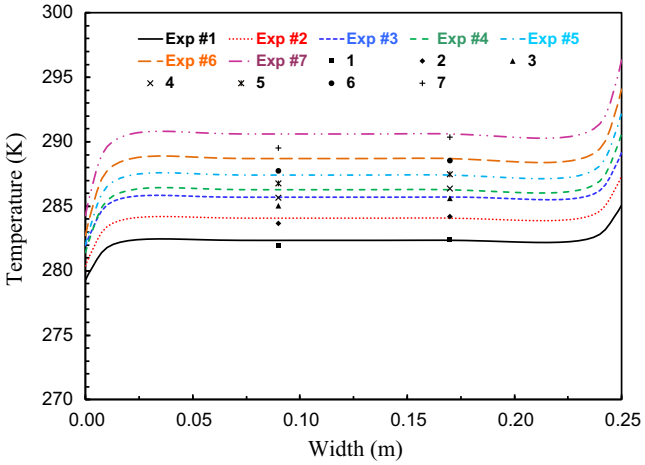

Fig. 15. The temperature distributions along the cavity width for different numerical experiments at y = 1.73 m.

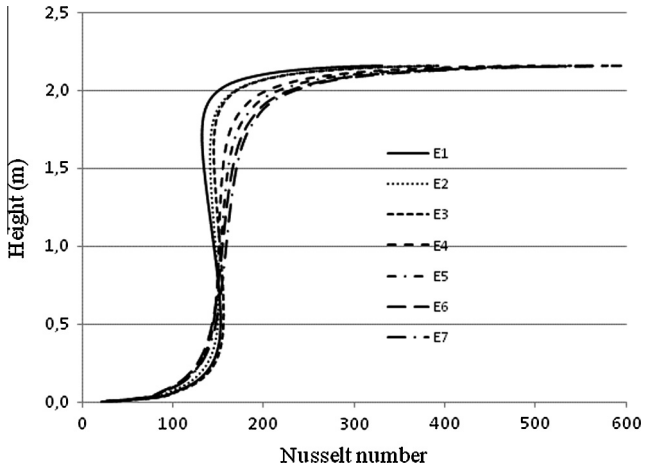

Fig. 17. Variations of the Nusselt numbers at the hot surface along the cavity height for different numerical experiments.

The Nusselt number distributions at the hot surface along the cavity height are shown in Fig. 17. The average Nusselt number increased with increasing Rayleigh number and reached the maximum value at the top of the cavity. Because of the restricted heat transfer at the bottom of the cavity, the Nusselt numbers start from the minimum values; throughout the cavity, there is no large difference between the Nusselt values as there was for the Rayleigh numbers.

The average Nusselt numbers for each experimental case are given in Table 2 for the hot surface of the cavity. The Nusselt number increases with buoyancy forces that are created by the temperature differences of the surface and air, which is induced by the density gradients.

These non-dimensional variables are introduced in the governing equations, and the velocity and temperature variations in the cavity arise in terms of the Nusselt and Rayleigh numbers. The results can be generalized by a correlation to predict the heat transfer rate using the Nusselt number for the double skin facade operating with the airproof condition and a Rayleigh number of approximately 10^{10}. Thus, the Nusselt number is a power function of the Rayleigh number,

Table 2
Average Nusselt numbers at the hot surface of the cavity for each experimental case.

Exp. number	#1	#2	#3	#4	#5	#6	#7
Nusselt numbers	142.6	147.7	152.5	156.5	160.9	165.2	168.8

$$Nu = C \cdot Ra^{m} \tag{11}$$

The Rayleigh and Nusselt numbers given in Tables 1 and 2 were used in a regression analysis to evaluate the indices C and m in Eq. (11); these values were calculated to be 0.082 and 0.325, respectively. Therefore, the correlation for the airproof cavity investigated in this study can be given as,

$$Nu = 0.082 \cdot Ra^{0.325} \tag{12}$$

The Nusselt and Rayleigh numbers for each case were drawn with the power function, as shown in Fig. 18. The coefficient of determination, R^2, was found to be 0.982, and the data fit well.

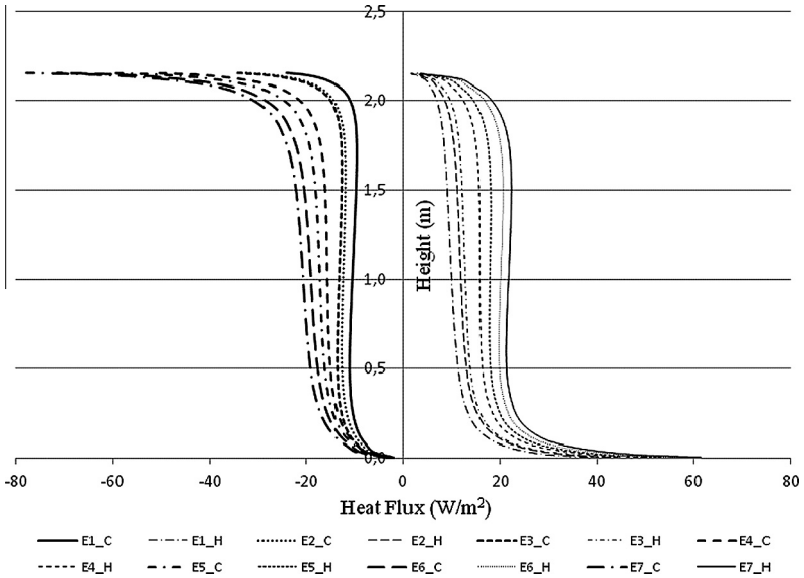

Fig. 16. Variations of the heat fluxes along the cavity height at the cold and hot surfaces for different numerical experiments.

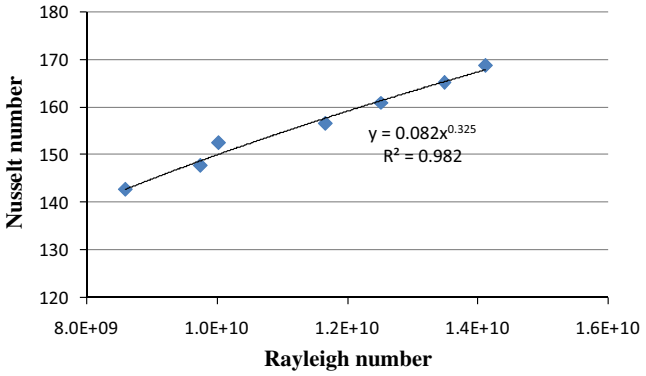

Fig. 18. Nusselt numbers as a function of Rayleigh numbers for the experimental case.

6. Conclusions

In this study, numerical and experimental studies were conducted to investigate the flow and heat transfer characteristics inside a double skin facade. A numerical model was developed to simulate the steady state natural convection inside a tall cavity. The comparative results show that the current model can successfully predict the velocity field and temperature variations inside the domain. The following conclusions can be obtained from the current study:

- The velocity field variations showed that increasing the temperature difference to approximately 65% did not cause a large difference in the working conditions.
- Even though the velocity field remained constant, the heat transfer increased by approximately 20% by increasing the temperature difference from 7 K to 11.8 K.
- A correlation was developed to predict the Nusselt numbers with the Rayleigh number ranging from $8.59 * 10^9$ to $1.41 * 10^{10}$ for an airproof double skin facade.

Future research should address the extension of the experimental and numerical analysis to different working conditions such as forced convection, geometric parameters, solar radiation loads, and time-dependent analysis using climatic data from different locations.

Acknowledgements

This study was supported by the Scientific and Technological Research Council of Turkey (TÜBİTAK) Foundation under Grant 112M170.

References

[1] X. Loncour, A. Deneyer, M. Blasco, G. Flament, P. Wouters, Ventilated Double Skin Façades Contributed Report 03, Belgian Building Research Institute (BBRI), 2004.
[2] G. De Vahl Davis, Laminar natural convection in an enclosed rectangular cavity, Int. J. Heat Mass Transf. 11 (1968) 1675–1693.
[3] M.W. Nansteel, R. Grief, Natural convection in enclosures with two- and three dimensional partitions, Int. J. Heat Mass Transf. 27 (1984) 561–571.
[4] K.J. King, Turbulent Natural Convection in Rectangular Air Cavities Ph.D. dissertation, Queen Mary College, University of London, 1989.
[5] Y.S. Tian, T.G. Karayiannis, Low turbulence natural convection in an air filled square cavity. Part I. Thermal and fluid flow fields, Int. J. Heat Mass Transf. 43 (2000) 849–866.
[6] Y.S. Tian, T.G. Karayiannis, Low turbulence natural convection in an air filled square cavity. Part II. The turbulence quantities, Int. J. Heat Mass Transf. 43 (2000) 867–884.
[7] P.L. Betts, I.H. Bokhari, Experiments on turbulent natural convection in an enclosed tall cavity, Int. J. Heat Fluid Flow 21 (6) (2000) 675–683.
[8] J. Salat, S. Xin, P. Joubert, A. Sergent, F. Penot, P. Le Quéré, Experimental and numerical investigation of turbulent natural convection in a large air-filled cavity, Int. J. Heat Fluid Flow (2004) 824–832.
[9] S.K. Choi, E.K. Kim, M.W. Wi, S.O. Kim, Computation of a turbulent natural convection in a rectangular cavity with the low-reynolds-number differential stress and flux model, KSME Int. J. 18 (10) (2004) 1782–1798.
[10] F.X. Trias, A. Gorobets, M. Soria, A. Oliva, Direct numerical simulation of a differentially heated cavity of aspect ratio 4 with Rayleigh numbers up to 10^{11}—Part I: Numerical methods and time-averaged flow, Int. J. Heat Mass Transf. 53 (4) (2010) 665–673.
[11] F.X. Trias, A. Gorobets, M. Soria, A. Oliva, Direct numerical simulation of a differentially heated cavity of aspect ratio 4 with Rayleigh numbers up to 10^{11}—Part II: Heat transfer and flow dynamics, Int. J. Heat Mass Transf. 53 (4) (2010) 674–683.
[12] D. Saury, N. Rouger, F. Djanna, F. Penot, Natural convection in an air-filled cavity: experimental results at large Rayleigh numbers, Int. Commun. Heat Mass Transfer 38 (2011) 679–687.
[13] G.E. Lau, G.H. Yeoh, V. Timchenko, J.A. Reizes, Application of dynamic global-coefficient subgrid-scale models to turbulent natural convection in an enclosed tall cavity, Phys. Fluids 24 (2012).
[14] H. Manz, Total solar energy transmittance of glass double façades with free convection, Energy Build. 36 (2) (2004) 127–136.
[15] M. Fossa, C. Menezo, E. Leonardi, Experimental natural convection on vertical surfaces for building integrated photovoltaic (BIPV) applications, Exp. Thermal Fluid Sci. 32 (4) (2008) 980–990.
[16] A. Pappas, Z. Zhai, Numerical investigation on thermal performance and correlations of double skin façade with buoyancy-driven airflow, Energy Build. 40 (4) (2008) 466–475.
[17] F. Kuznik, T. Catalina, L. Gauzere, M. Woloszyn, J.J. Roux, Numerical modelling of combined heat transfers in a double skin façade- Full scale laboratory experiment validation, Appl. Therm. Eng. 31 (2011) 3043–3054.
[18] W. Pasut, M. De Carli, Evaluation of various CFD modelling strategies in predicting airflow and temperature in a naturally ventilated double skin façade, Appl. Therm. Eng. 37 (2012) 267–274.
[19] J. Xaman, G. Alvarez, L. Lira, C. Estrada, Numerical study of heat transfer by laminar and turbulent natural convection in tall cavities of facade elements, Energy Build. 37 (7) (2005) 787–794.
[20] A. Missoum, M. Elmir, A. Belkacema, M. Naboua, B. Draouia, Numerical simulation of heat transfer through a double-walled facade building in arid zone, Energy Proc. 36 (2013) 834–843.
[21] ANSYSInc, ANSYS-FLUENT 14.0 Theory Guide, 2009.
[22] S.V. Patankar, Numerical Heat Transfer and Fluid Flow, Hemisphere, Washington, D.C., 1980.
[23] B.P. Leonard, S. Mokhtari, ULTRA-SHARP Nonoscillatory Convection Schemes for High-Speed Steady Multidimensional Flow, NASA TM 1-2568 (ICOMP-90-12), NASA Lewis Research Center, 1990.